Efficient generation of THz pulses with 0.4 mJ energy

J. A. Fülöp,[1,5,*] Z. Ollmann,[2,5] Cs. Lombosi,[2,5] C. Skrobol,[3,4] S. Klingebiel,[3] L. Pálfalvi,[2] F. Krausz,[3,4] S. Karsch,[3,4] and J. Hebling[1,2,5]

[1]*MTA-PTE High-Field Terahertz Research Group, Ifjúság ú. 6, 7624 Pécs, Hungary*
[2]*Institute of Physics, University of Pécs, Ifjúság ú. 6, 7624 Pécs, Hungary*
[3]*Max-Planck-Institut für Quantenoptik, Hans-Kopfermann-Str. 1, 85748 Garching, Germany*
[4]*Department für Physik, Ludwig-Maximilians-Universität München, Am Coulombwall 1, 85748 Garching, Germany*
[5]*Szentágothai Research Centre, University of Pécs, Ifjúság ú. 20, 7624 Pécs, Hungary*
[*]*fulop@fizika.ttk.pte.hu*

Abstract: Efficient generation of THz pulses with high energy was demonstrated by optical rectification of 785-fs laser pulses in lithium niobate using tilted-pulse-front pumping. The enhancement of conversion efficiency by a factor of 2.4 to 2.7 was demonstrated up to 186 μJ THz energy by cryogenic cooling of the generating crystal and using up to 18.5 mJ/cm^2 pump fluence. Generation of THz pulses with more than 0.4 mJ energy and 0.77% efficiency was demonstrated even at room temperature by increasing the pump fluence to 186 mJ/cm^2. The spectral peak is at about 0.2 THz, suitable for charged-particle manipulation.

OCIS codes: (190.0190) Nonlinear optics; (300.6495) Spectroscopy, terahertz; (160.3730) Lithium niobate.

References and Links

1. J. Hebling, M. C. Hoffmann, H. Y. Hwang, K.-L. Yeh, and K. A. Nelson, "Observation of nonequilibrium carrier distribution in Ge, Si, and GaAs by terahertz pump–terahertz probe measurements," Phys. Rev. B **81**(3), 035201 (2010).
2. S. Fleischer, Y. Zhou, R. W. Field, and K. A. Nelson, "Molecular orientation and alignment by intense single-cycle THz pulses," Phys. Rev. Lett. **107**(16), 163603 (2011).
3. B. Schütte, U. Frühling, M. Wieland, A. Azima, and M. Drescher, "Electron wave packet sampling with laser-generated extreme ultraviolet and terahertz fields," Opt. Express **19**(20), 18833–18841 (2011).
4. T. Kampfrath, K. Tanaka, and K. A. Nelson, "Resonant and nonresonant control over matter and light by intense terahertz transients," Nat. Photon. **7**(9), 680–690 (2013).
5. J. Hebling, J. A. Fülöp, M. I. Mechler, L. Pálfalvi, C. Tőke, and G. Almási, "Optical manipulation of relativistic electron beams using THz pulses," arXiv:1109.6852 (2011).
6. L. J. Wong, A. Fallahi, and F. X. Kärtner, "Compact electron acceleration and bunch compression in THz waveguides," Opt. Express **21**(8), 9792–9806 (2013).
7. L. Pálfalvi, J. A. Fülöp, G. Tóth, and J. Hebling, "Evanescent-wave proton postaccelerator driven by intense THz pulse," Phys. Rev. ST Accel. Beams **17**(3), 031301 (2014).
8. E. Balogh, K. Kovács, P. Dombi, J. A. Fülöp, G. Farkas, J. Hebling, V. Tosa, and K. Varju, "Single attosecond pulse from terahertz-assisted high-order harmonic generation," Phys. Rev. A **84**(2), 023806 (2011).
9. K. Kovács, E. Balogh, J. Hebling, V. Toşa, and K. Varjú, "Quasi-phase-matching high-harmonic radiation using chirped THz pulses," Phys. Rev. Lett. **108**(19), 193903 (2012).
10. T. Plettner, P. P. Lu, and R. L. Byer, "Proposed few-optical cycle laser-driven particle accelerator structure," Phys. Rev. ST Accel. Beams **9**(11), 111301 (2006).
11. E. A. Peralta, K. Soong, R. J. England, E. R. Colby, Z. Wu, B. Montazeri, C. McGuinness, J. McNeur, K. J. Leedle, D. Walz, E. B. Sozer, B. Cowan, B. Schwartz, G. Travish, and R. L. Byer, "Demonstration of electron acceleration in a laser-driven dielectric microstructure," Nature **503**(7474), 91–94 (2013).
12. A. Sell, A. Leitenstorfer, and R. Huber, "Phase-locked generation and field-resolved detection of widely tunable terahertz pulses with amplitudes exceeding 100 MV/cm," Opt. Lett. **33**(23), 2767–2769 (2008).
13. C. P. Hauri, C. Ruchert, C. Vicario, and F. Ardana, "Strong-field single-cycle THz pulses generated in an organic crystal," Appl. Phys. Lett. **99**(16), 161116 (2011).
14. H. Hirori, A. Doi, F. Blanchard, and K. Tanaka, "Single-cycle terahertz pulses with amplitudes exceeding 1 MV/cm generated by optical rectification in $LiNbO_3$," Appl. Phys. Lett. **98**(9), 091106 (2011).

#212542 - $15.00 USD Received 23 May 2014; revised 14 Jul 2014; accepted 21 Jul 2014; published 12 Aug 2014

15. A. G. Stepanov, L. Bonacina, S. V. Chekalin, and J.-P. Wolf, "Generation of 30 microJ single-cycle terahertz pulses at 100 Hz repetition rate by optical rectification," Opt. Lett. **33**(21), 2497–2499 (2008).
16. J. A. Fülöp, L. Pálfalvi, S. Klingebiel, G. Almási, F. Krausz, S. Karsch, and J. Hebling, "Generation of sub-mJ terahertz pulses by optical rectification," Opt. Lett. **37**(4), 557–559 (2012).
17. S.-W. Huang, E. Granados, W. R. Huang, K.-H. Hong, L. E. Zapata, and F. X. Kärtner, "High conversion efficiency, high energy terahertz pulses by optical rectification in cryogenically cooled lithium niobate," Opt. Lett. **38**(5), 796–798 (2013).
18. C. Vicario, B. Monoszlai, C. Lombosi, A. Mareczko, A. Courjaud, J. A. Fülöp, and C. P. Hauri, "Pump pulse width and temperature effects in lithium niobate for efficient THz generation," Opt. Lett. **38**(24), 5373–5376 (2013).
19. J. Hebling, G. Almasi, I. Z. Kozma, and J. Kuhl, "Velocity matching by pulse front tilting for large area THz-pulse generation," Opt. Express **10**(21), 1161–1166 (2002).
20. J. A. Fülöp, L. Pálfalvi, G. Almási, and J. Hebling, "Design of high-energy terahertz sources based on optical rectification," Opt. Express **18**(12), 12311–12327 (2010).
21. J. A. Fülöp, L. Pálfalvi, M. C. Hoffmann, and J. Hebling, "Towards generation of mJ-level ultrashort THz pulses by optical rectification," Opt. Express **19**(16), 15090–15097 (2011).
22. M. I. Bakunov, S. B. Bodrov, and E. A. Mashkovich, "Terahertz generation with tilted-front laser pulses: dynamic theory for low-absorbing crystals," J. Opt. Soc. Am. B **28**(7), 1724–1734 (2011).
23. S. Klingebiel, C. Wandt, C. Skrobol, I. Ahmad, S. A. Trushin, Zs. Major, F. Krausz, and S. Karsch, "High energy picosecond Yb:YAG CPA system at 10 Hz repetition rate for pumping optical parametric amplifiers," Opt. Express **19**(6), 5357–5363 (2011).
24. Y. Shen, T. Watanabe, D. A. Arena, C.-C. Kao, J. B. Murphy, T. Y. Tsang, X. J. Wang, and G. L. Carr, "Nonlinear cross-phase modulation with intense single-cycle terahertz pulses," Phys. Rev. Lett. **99**(4), 043901 (2007).
25. S. A. Ku, C. M. Tu, W.-C. Chu, C. W. Luo, K. H. Wu, A. Yabushita, C. C. Chi, and T. Kobayashi, "Saturation of the free carrier absorption in ZnTe crystals," Opt. Express **21**(12), 13930–13937 (2013).
26. L. Pálfalvi, J. A. Fülöp, G. Almási, and J. Hebling, "Novel setups for extremely high power single-cycle terahertz pulse generation by optical rectification," Appl. Phys. Lett. **92**(17), 171107 (2008).
27. K. Nagashima and A. Kosuge, "Design of rectangular transmission gratings fabricated in $LiNbO_3$ for high-power terahertz-wave generation," Jpn. J. Appl. Phys. **49**(12), 122504 (2010).
28. Z. Ollmann, J. Hebling, and G. Almási, "Design of a contact grating setup for mJ-energy THz pulse generation by optical rectification," Appl. Phys. B **108**(4), 821–826 (2012).

1. Introduction

The development of intense THz sources in the last few years enabled many new applications, thereby opening up the realm of THz-pulse-induced nonlinear phenomena. Typically, μJ-level THz pulse energies and peak electric field strengths on the order of 100 kV/cm are required for these studies. THz pump—THz probe measurements were successfully used to gain new insight into ultrafast carrier dynamics of semiconductors [1]. Intense THz fields were also used for field-free orientation and alignment of molecules [2] and for electron wave packet sampling (streaking) [3]. These and many other remarkable results of recent THz-induced nonlinear studies clearly show the discovery and application potential of intense THz pulses [4].

An emerging group of interesting new applications, including especially the manipulation of charged particles and charged-particle beams, will require THz pulses with extremely high energy and peak electric field strength up to the multi-mJ and muti-10-MV/cm level, respectively. Examples are acceleration, longitudinal compression, and undulation of relativistic electron bunches [5,6], which can lead to single- or few-cycle femtosecond-attosecond pulse generation, or the post-acceleration of laser-generated proton and ion beams with potential applications for hadron therapy [7]. Further application possibilities are investigations of material properties and processes under the influence of extremely high THz fields, multispectral single-shot imaging, THz-enhanced attosecond-pulse generation with increased cut-off frequency [8] and efficiency in a quasi-phase-matched scheme [9]. The important advantage of the low-frequency (0.1 to 3 THz) part of THz spectrum over visible or infrared laser pulses [10,11] is the longer wavelength ideally matching typical transversal sizes of particle beams, being on the order of 10 to 100 μm. The advantage of THz radiation over microwaves is the easier possibility of high-precision, low-jitter synchronization and the higher achievable field strength.

#212542 - $15.00 USD Received 23 May 2014; revised 14 Jul 2014; accepted 21 Jul 2014; published 12 Aug 2014

At present extremely high field strengths up 100 MV/cm are available only in the higher-frequency part (above 10 THz) of the THz spectrum [12]. The energy and peak electric field of presently available intense table-top sources in the low-frequency THz range is one or two orders of magnitude below the required level [13–18]. In this spectral range, both the highest energy (125 μJ) [16] and efficiency (3.8%) [17] obtained by optical rectification (OR) of fs-ps laser pulses were demonstrated with tilted-pulse-front pumping (TPFP) [19] in lithium niobate ($LiNbO_3$, LN). The key aspect in this recent development of high-energy and efficient THz sources was to optimize the Fourier-limited (FL) pump pulse duration and to cool LN to cryogenic temperature (CT) to reduce its THz absorption, as proposed and predicted by theoretical studies [20–22]. The calculations indicated about 500 fs as the optimal FL pump pulse duration in LN [21]. This is much longer than the typically used ~100 fs.

Here we present experimental results showing substantial increase of the THz pulse energy beyond 0.4 mJ, generated with high efficiency by OR of femtosecond laser pulses in LN using TPFP. To our knowledge, this is the highest THz pulse energy reported so far from OR. The key aspect is to use close-to-optimal pump pulse duration. Another key aspect of efficient generation of high-energy THz pulses is the cryogenic cooling of LN. We present experimental results showing the enhancement of conversion efficiency at CT to more than 0.18 mJ THz energy. The characterization of high-energy THz pulses by electro-optic sampling (EOS) and focal spot measurement is also shown.

The paper is organized as follows. Section 2 describes the experimental setup and methods in detail. In Sec. 3 the experimental results are presented for various setup configurations and a detailed discussion is given. Conclusions are drawn in Sec. 4.

2. Experimental setup

A diode-pumped high-energy picosecond Yb:YAG chirped-pulse amplification system was used as the pump laser with 10 Hz repetition rate, 1030 nm central wavelength, and 3.4 nm FWHM spectral bandwidth [23]. The pulses were compressed to about 785 fs duration containing a small remaining third- and higher-order spectral phase. This pump pulse duration is longer than the predicted ~500 fs optimum for THz generation in LN, but is still close to it. The amplitude and phase structure of the pump pulses were characterized by a single-shot SHG FROG apparatus. The pump beam diameter was 26 mm (FWHM). Up to about 60 mJ energy was used in the experiment.

An overview of the different experimental conditions and the achieved maximum THz yield is given in Table 1. For the generation of the highest THz energies the intensity front of the pump pulses was tilted by a 1400-lines/mm grating (Setup 1, Fig. 1(a)). A λ/2 plate was used to rotate the horizontally polarized pump light diffracted from the grating to vertical polarization, parallel to the optic axis of the LN crystal. Optimal imaging conditions [20] were provided by a telescope consisting of one 25-cm focal-length, 50-mm diameter and one 15-cm focal-length, 25-mm diameter lenses in confocal arrangement, and a vacuum tube in between them to avoid nonlinear effects in air. Latter prohibited plasma formation in the focal plane of the first lens and the onset of nonlinear beam distortions in air. A 0.6% MgO-doped stoichiometric LN prism at room temperature (RT) with a useful input surface of 8.1 × 16 mm^2 (horizontal × vertical) was used for OR. An additional 2.5:1 demagnifying telescope was used in front of the TPFP setup to reduce the incoming pump beam diameter and to achieve high pump intensities at LN. The pumped area (A) on the crystal surface was relatively small, its diameter was 5.7 mm in the horizontal direction and 7.0 mm in the vertical direction (Table 1); both values refer to full width at half-maximum (FWHM).

#212542 - $15.00 USD Received 23 May 2014; revised 14 Jul 2014; accepted 21 Jul 2014; published 12 Aug 2014

Table 1. Overview of the different experimental conditions used in the measurements, and the achieved maximum THz energies and efficiencies. The mean pump fluence and intensity were calculated using FWHM values for both spot size and pulse duration. Throughout the paper we refer to LN temperature, pumped area, and the type of imaging optics in plot legends.

setup			pump			THz	
LN temperature [K]	pumped spot diameter [mm × mm]	imaging	max. energy [mJ]	max. fluence [mJ/cm^2]	max. intensity [GW/cm^2]	max. energy [μJ]	max. efficiency [%]
300 (RT)	5.7 × 7.0 (small *A*)	telescope	56.9	186	237	436	0.77
300 (RT)	8.1 × 15.3 (large *A*)	lens	30.0	18.5	23.6	68.3	0.23
23 (CT, average)						186	0.62

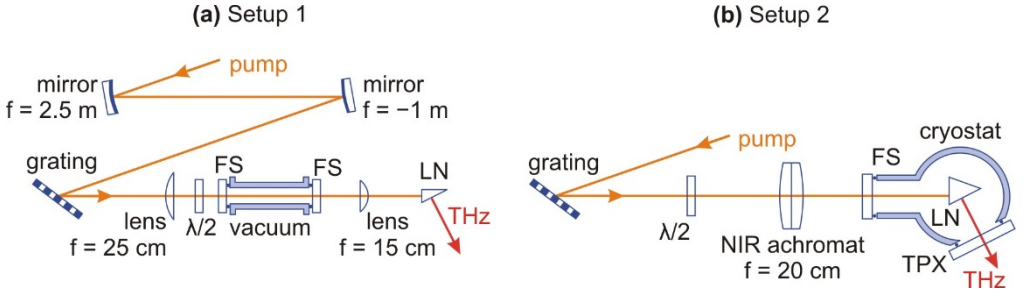

Fig. 1. Different TPFP setups used in the experiments: (a) Setup 1 with beam-narrowing and imaging telescopes; (b) Setup 2 with the near-infrared achromat lens. FS: fused silica window, NIR: near-infrared.

Another TPFP setup was used to compare high-energy THz pulse generation at RT and CT (Setup 2, Fig. 1(b), see also Table 1). To enable easier adjustment of the pulse-front tilt angle for velocity matching, which changes with temperature, we replaced the imaging telescope by a 20 cm focal length, 50 mm diameter near-infrared achromat lens. A 0.6% MgO-doped stoichiometric LN prism with 8.1 × 20 mm^2 (horizontal × vertical) useful input surface was used. The FWHM pump spot size at the crystal surface was large, 10.4 mm in the horizontal direction (out of which 8.1 mm was effective) and 15.3 mm in the vertical direction (Table 1). The LN crystal was placed inside a closed-cycle helium cryostat (Model 22 from Cryodyne) with a fused silica input window for the pump and a polymethylpentene (TPX) exit window for THz. The vacuum chamber of the cryostat was evacuated to about 10^{-6} mbar. The chamber had an elongated input port (with the FS window) for the pump beam in order to accommodate the focus of the NIR achromat lens in vacuum to avoid nonlinear effects in air. The LN crystal was placed on a small Al table holder attached to the cold finger of the cryostat. Measurements were done at RT (300 K) and CT (23 K).

A calibrated pyroelectric detector (Microtech Instruments) with 2 × 3 mm^2 active area and a cone-shaped metallic input opening with 15 mm diameter was used for measuring the energy of the THz pulses. A silicon wafer of 0.5 mm thickness with 70% measured transmission and a cardboard plate with 80% transmission were placed in front of the detector to block the optical radiation (the fundamental pump and its second harmonic). In some cases additional cardboard plates were used to further attenuate the THz pulses in order to avoid saturation of the detector. In each case the transmission of the filter assembly was carefully measured. The voltage signal of the detector was fed to a storage oscilloscope and the THz energy W_{THz} was calculated from the voltage modulation V_{m} of the recorded trace according to $W_{\mathrm{THz}} = C \cdot V_{\mathrm{m}} \cdot \tau / S$, where the sensitivity S = 700 V/W was obtained from factory calibration, while the correction factor $C \approx 1$ and the time constant τ = 25 ms were determined from fitting of the recorded trace [16].

#212542 - $15.00 USD Received 23 May 2014; revised 14 Jul 2014; accepted 21 Jul 2014; published 12 Aug 2014

The THz beam emerging from the LN source was collimated by a 6-inch effective-focal-length (EFL), 2-inch diameter, 90° deviation off-axis parabolic (OAP) mirror and focused by a 2-inch EFL, 2-inch diameter, 90° OAP. The focal spot size was measured by the knife-edge technique. For measuring the temporal waveform by EOS of the THz pulses the knife edge was replaced by a 0.1 mm thick (110)-cut ZnTe plate, attached to a 1 mm thick inactive ZnTe substrate. Two wiregrid polarizers were used to attenuate the THz beam in the collimated section to avoid the over-rotation of the induced birefringence in ZnTe [24]. A small, apertured fraction of the pump beam (the 0-order reflection from the grating) was taken as the probe for EOS. Due to space constraints in the setup we have used reflection-type EOS geometry, where THz and pump entered the detector crystal from opposite directions. It was the probe reflected internally from the outside surface of the active layer that co-propagated with THz, and which was detected. The EOS signal was recorded by balanced detection consisting of a quarter-wave plate, a Wollaston prism, and two photodiodes. A lock-in amplifier with 10 Hz reference signal and 300 ms long integration time (i.e. averaging over 3 pulses) was used to improve the signal-to-noise ratio.

3. Results and discussion

3.1 THz pulses with more than 0.4 mJ energy

The main goal of our experiment was to increase the THz pulse energy to the highest possible value. We used the TPFP setup with the imaging telescope (Setup 1, Fig. 1(a)) since our ray-tracing calculations predicted smaller curvature of the tilted pulse front than that with single-lens imaging. This feature is beneficial for achieving high conversion efficiency with large (cm-scale) pumped area. As mentioned in Sec. 2, the pumped spot size was 5.7 mm × 7.0 mm (horizontal × vertical).

The measured THz energy at RT is shown in Fig. 2(a) as function of the pump energy (bottom scale) and intensity (top scale) measured directly before entering the LN crystal. The maximum pump energy was 58 mJ, the maximum intensity 237 GW/cm^2 (see also Table 1). Monotonic increase of the THz energy with increasing pump energy can be observed in the entire range. We note that this behavior is distinctly different from our previous observation using significantly longer (1.3 ps) pump pulses but similar (only 23% smaller) pumped area [16], where the THz energy started to decrease above 45 mJ pump energy (Fig. 2(a)). By fitting power functions to the measured data in different pump energy ranges (lines in Fig. 2(a)) one sees a decreasing power exponent with increasing pump energy. It is about 1.5 below 10 mJ and 1.4 in the range of 10 mJ to 30 mJ. Interestingly, above 30 mJ the exponent rises to almost 1.7. To explore the reason for this effect requires further investigation, which is out of the scope of the present study. However, we would like to call into attention that similar behavior was observed in ZnTe and was explained by the saturation of free-carrier absorption at higher pump intensities [25]. Such an effect may also play a role in case of LN.

#212542 - $15.00 USD Received 23 May 2014; revised 14 Jul 2014; accepted 21 Jul 2014; published 12 Aug 2014

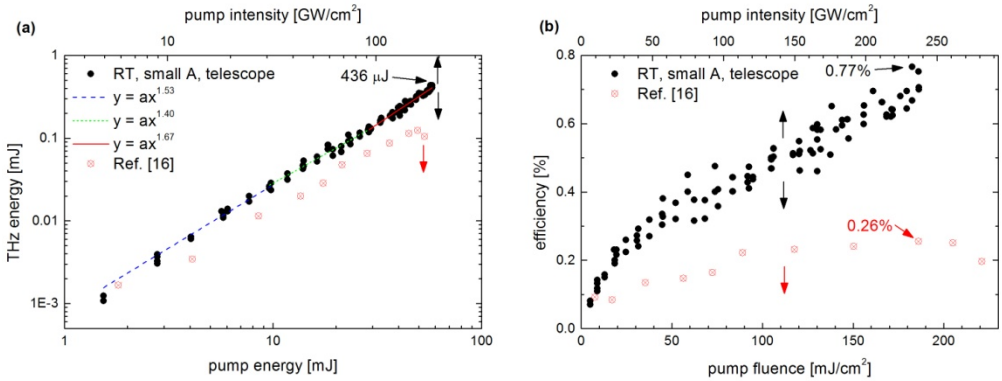

Fig. 2. Measured THz energy vs. pump energy and intensity (a), and the corresponding efficiencies vs. pump fluence and intensity (b). Empty red symbols are from our previous experiment [16]. Both intensity scales refer only to the present experiment, as indicated by arrows.

The maximum THz energy achieved in the present experiment was as high as 436 μJ achieved with only 58 mJ pump energy. Corresponding pump-to-THz energy conversion efficiencies up to 0.77% were observed (Fig. 2(b)). Measured efficiencies are shown in Fig. 2(b) as function of the pump fluence (for better comparison with results from our previous experiment [16]) and intensity. It is monotonically increasing with increasing energy in the entire range. Above about 80 mJ/cm^2 fluence (corresponding to about 25 mJ energy) it is increasing linearly. Up to about 150 mJ/cm^2 (47 mJ), the saturation point of our previous measurement, we obtained about two times higher efficiencies with the presently used shorter pump pulses than with 1.3 ps pulses. This is in good agreement with our previous calculations [16], which predict 2.3-times increase for the shorter pump pulses being closer to optimum.

3.2 Enhancement of high-energy THz pulse generation at low temperatures

It was predicted by calculations that the THz generation efficiency (η) can be enhanced by a factor of 3 to 6 when the LN crystal is cooled to CT [21]; the exact value depends on pump pulse duration and temperature. For 785 fs pump pulses an efficiency-enhancement factor of $\eta_{CT}/\eta_{RT} \approx 3$ to 4 can be expected. With a dedicated measurement series, our goal was to investigate this effect for 100 μJ-level THz pulse energies; that is, for energies much higher than that used in previous experimental studies [17,18].

Since cooling LN from RT to CT results in a small but significant change of the pulse-front-tilt angle, required for pump-THz velocity matching, it is necessary to adjust this angle. This can easily be done in a TPFP setup containing one single imaging lens by slightly shifting the lens (with a telescope one would have to change the input beam direction). For this reason in the temperature-dependent measurements we used Setup 2, i.e. TPFP with a single lens and large pumped area (see Sec. 2). The maximum useful pump energy was 30 mJ, the maximum intensity was 23.6 GW/cm^2.

The measured THz energies at RT and CT are shown in Fig. 3(a) as function of the useful pump energy and intensity. Continuous increase of the THz energy can be observed for both temperatures in the entire range. The maximum THz energy is about 2.7-times higher at CT (186 μJ) than at RT (68 μJ), which is in good agreement with calculations [21]. This increase is due to the reduced absorption of LN at CT [21]. The fitted power exponent (Fig. 3(a)) decreases again with pump energy from 1.8 below 10 mJ to 1.5 above 20 mJ at CT and from 1.8 to 1.3 at RT. Figure 3(b) shows the corresponding pump-to-THz energy conversion efficiencies as functions of the useful pump energy and intensity. The conversion efficiencies are increasing with pump energy up to about 15 mJ (12 GW/cm^2 intensity). Above this level the efficiencies increase at reduced rates. The maximum measured efficiencies were 0.62%

#212542 - $15.00 USD Received 23 May 2014; revised 14 Jul 2014; accepted 21 Jul 2014; published 12 Aug 2014

(CT) and 0.23% (RT). The ratio η_{CT}/η_{RT} of the CT and RT efficiencies (empty symbols in Fig. 3(b)) is about 2.7 below about 15 mJ pump energy (12 GW/cm^2 intensity). This value is slightly smaller but close to that predicted by calculations. A pronounced drop of the efficiency enhancement factor to less than 2.4 can be observed in the narrow range between 15 and 20 mJ pump energies (12 GW/cm^2 and 16 GW/cm^2 intensities). The origin of this behavior needs further investigation. At higher energies the enhancement factor increases slowly from about 2.4 to 2.6.

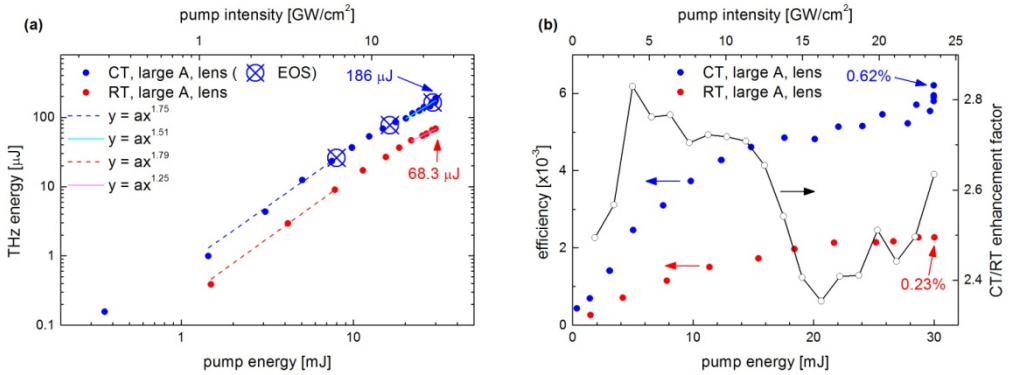

Fig. 3. (a) Measured THz energy vs. pump energy and intensity at RT and CT. The large crossed symbols refer to measurement points where electro-optic sampling was also carried out (see Sec. 3.3). (b) The corresponding conversion efficiencies vs. pump energy and intensity at CT and RT. The ratio of the CT and RT efficiencies, obtained by interpolation, is shown by the empty symbols.

3.3 Characterization of high-energy THz pulses

Key characteristics of high-energy THz pulses important for applications are the pulse energy, the temporal waveform, the corresponding spectrum, and the focusability of the THz beam. These parameters also determine the achievable focused peak electric field. In order to characterize these important features for our high-energy THz pulses, we carried out EOS and focal spot measurements, in addition to the energy measurements shown in Sec. 3.2. THz pulses were generated with Setup 2, i.e. using CT, large pumped area, and a single lens for imaging (see Secs. 2 and 3.2).

Examples of measured in-focus waveforms are shown in Fig. 4(a) for three different THz pulse energies: W_{THz} = 26 μJ, 77 μJ, and 163 μJ, which correspond to 7.8 mJ, 16 mJ, and 29 mJ pump energies, respectively (see also Fig. 3(a)). The waveforms are strongly asymmetric, comprised of less than one full oscillation cycle, with one dominating half-cycle. They show positive chirp, with the low frequencies coming early. We note that the relatively strong noise mainly comes from the low repetition rate of the laser. A pronounced shift of the mean frequency to lower values with increasing THz pulse energy can be anticipated from the waveforms. There is also an increasing delay in the time instant of the peak position with increasing THz energy. The peak electric field strengths are 0.26 MV/cm, 0.45 MV/cm, and 0.65 MV/cm, as calculated from the measured waveform, pulse energy, and focal spot size (for latter see the last paragraph of this Sec.). We note that it is important to take into account the low THz frequencies in our experiment when comparing these peak amplitudes to those in other experiments [12–14]. To our knowledge, in the low-frequency range accessed in our experiment (see also the next paragraph), the measured electric fields are the highest ones reported so far.

#212542 - $15.00 USD Received 23 May 2014; revised 14 Jul 2014; accepted 21 Jul 2014; published 12 Aug 2014

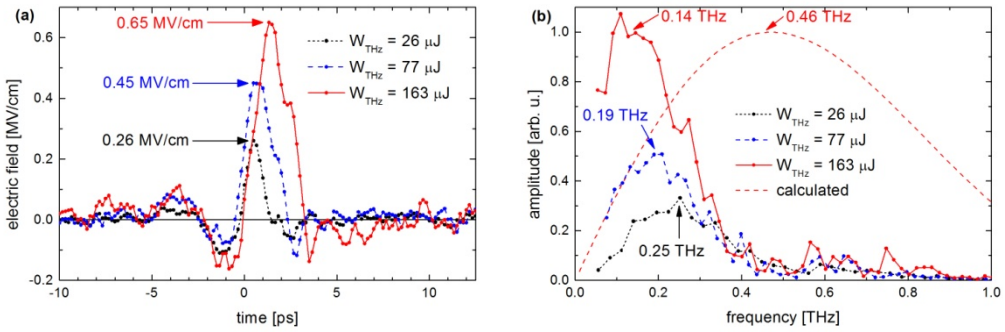

Fig. 4. (a) Focused electric field waveforms measured by EOS. (b) Spectral amplitudes obtained from measured waveforms by Fourier transformation, in comparison with the calculated spectrum.

The spectral amplitudes of the THz pulses, obtained by Fourier transformation from the measured waveforms, are shown in Fig. 4(b). In all cases the spectra extend up to about 1 THz. They consist of an intense low-frequency part, extending up to about 0.4 THz, and an adjoining weak part, with about one order of magnitude smaller spectral amplitude, extending up to about 1 THz. We note that similar spectral distribution was observed in our previous experiment with much smaller pump pulse energies [18]. Simulations based on the model described in our previous work [20] show somewhat broader spectra extending beyond 1 THz, however with the usual more uniform distribution (dashed curve without symbols in Fig. 4(b)) without any drop at around 0.4 THz. Another interesting feature is the decreasing frequency of the spectral peak with increasing pump and THz energy. It is about 0.25 THz for 26 μJ THz energy, which reduces nearly to its half, 0.14 THz, for 163 μJ. In the simulation, no energy dependence of the THz spectra is present. In contrast to the peak frequency, the widths of the observed spectra show no significant energy-dependence, neither for the entire spectra nor for the more intense low-frequency parts. Gaussian fit to the latter gives spectral FWHMs varying in the 0.27 THz to 0.24 THz range. The reason for the observed spectral features needs further dedicated investigation beyond the scope of the present work, possibly including the role of impurities in the LN crystal, as well as pump- and THz-induced nonlinear effects.

The focal spot size was measured by the knife-edge method for the highest (29 mJ) pump energy. The measured THz energies as function of the knife edge position are shown in Fig. 5 both for horizontal and vertical scans. The fitted curves correspond to the assumption of an elliptical Gaussian beam, and coincide well with the measured data points. The fit gives $1/e^2$-radii of w_H = 2.4 mm in the horizontal, and w_V = 2.7 mm in the vertical directions. A little astigmatism was observed, the horizontal and vertical foci being about 5 mm apart. We also carried out a measurement of the unfocused THz beam profile in the horizontal direction at various distances from the LN crystal. The THz beam size and wavefront curvature directly behind the LN crystal could be estimated from a fit to the measured profiles. Gaussian beam calculation starting from these fitted values gave $w_{H,calc}$ = 2.0 mm for the horizontal focal spot radius, which is only slightly smaller than the measured w_H = 2.4 mm value. The astigmatism can be attributed to the different THz wavefront curvatures in the horizontal and vertical directions, which is due to imaging errors [20]. To eliminate this effect and get closer to a diffraction-limited focal spot, thereby increasing the THz field strength, the aberration-free contact-grating technique [26] may be used.

#212542 - $15.00 USD Received 23 May 2014; revised 14 Jul 2014; accepted 21 Jul 2014; published 12 Aug 2014

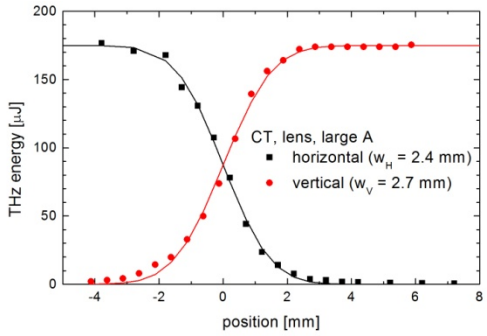

Fig. 5. Focal spot size measurement by knife-edge scan. The fitted curves correspond to assuming elliptical Gaussian intensity profile.

4. Conclusion

Efficient generation of THz pulses with high energy was demonstrated by optical rectification of 785-fs laser pulses in lithium niobate using tilted-pulse-front pumping. Enhancement of the THz generation efficiency at CT by 2.4- to 2.7-times over that at RT was shown up to 186 μJ THz energy by using up to 18.5 mJ/cm^2 pump fluence. Single-cycle/sub-cycle waveforms with spectral peaks around 0.2 THz were measured. The generation of THz pulses with more than 0.4 mJ energy and 0.77% efficiency was demonstrated by increasing the pump fluence up to 186 mJ/cm^2. The achieved THz pulse energies are, to our knowledge, the highest values reported for optical rectification (almost 3.5-times higher than the previously reported maximum [16]). Owing to the nearly optimal pump pulse duration, the achieved THz generation efficiency is the highest one measured at high THz energies.

Our measurements also revealed anomalies in THz power scaling and spectral shape, which can be important in designing highest-energy THz sources and applications in the near future and require further studies. The achieved high THz pulse energies and peak electric field strengths are suitable to access charged-particle manipulation and acceleration experiments in an optimally fitting THz frequency range.

Based on the presented results it can be expected that the THz energy will be increased beyond 1 mJ in the near future by using compact diode-pumped solid-state pump lasers with only 50 to 100 mJ pulse energy, optimal pulse duration and cryogenic cooling of LN. Multi-mJ THz pulses can be expected when combining these optimal conditions with the aberration-free contact-grating technique [26–28]. These developments will enable to realize one of the major application goals of the newly emerging high-field THz science: efficient and versatile manipulation and acceleration of charged particles and charged-particle beams.

Acknowledgments

Financial support from Hungarian Scientific Research Fund (OTKA) grant numbers 101846 and 113083, and the ELI_09-1-2010-0013 project is acknowledged.